Role of adiabaticity in controlling alkali-metal fine-structure mixing induced by rare gases

Ben Eshel,[*] Joseph A. Cardoza, David E. Weeks, and Glen P. Perram[†]

Department of Engineering Physics, Air Force Institute of Technology, 2950 Hobson Way, Wright-Patterson Air Force Base, Ohio 45433, USA

(Received 26 October 2016; published 20 April 2017; corrected 27 April 2017)

The collision cross sections for alkali-metal–rare-gas spin orbit mixing between the $n^2P_{3/2} \rightarrow n^2P_{1/2}$ levels trend strongly with the Massey parameter, or adiabaticity of the collisions. The strength of the interaction, as characterized by the C_6 dispersion coefficient, is a secondary influence on the rates. An analytic expression for the probability of energy transfer in alkali-metal–rare-gas collisions is derived using time-dependent perturbation theory. The model agrees well with a broad literature survey of the observed temperature-dependent cross sections. A simple interaction potential successfully organizes the alkali-metal–rare-gas database. The rates become very large for high-lying states, as the collisions are quite sudden and the radius of the valence electron is large. In contrast, the highly adiabatic cesium 6^2P mixing rates are six to eight orders of magnitude smaller. The mixing rate for the Rb-He diode pumped alkali laser system varies from 0.20–1.53 $\times 10^{-11}$cm^3/at. s for $T = 279$–893 K.

DOI: 10.1103/PhysRevA.95.042708

I. INTRODUCTION

The diode pumped alkali laser (DPAL) was introduced in 2003 by Krupke [1] and quickly became a system of great interest for high-power applications including laser weapons [2]. Diode laser bars are used to pump the $D_2\ ^2S_{1/2} \rightarrow\ ^2P_{3/2}$ transition, and collisional energy transfer to the spin-orbit split $^2P_{1/2}$ state yields lasing on the $D_1\ ^2P_{1/2} \rightarrow\ ^2S_{1/2}$ transition in potassium, rubidium, or cesium vapor. Multikilowatt lasers have been demonstrated [3,4], the intensity scaled to >7 MW/cm^2 [5–7], and performance models developed [8–10]. Scaling the output power and system efficiency depend critically on pressure broadening of the pump transition to optimize spectral overlap between the diode pump and atomic transition [11–15] and rapid collision-induced spin-orbit mixing [16–19] to prevent bottlenecking of the laser cycle. Cycle times as short as 74 ps have been achieved in potassium using helium only as the collision partner [5]. The spin-orbit mixing rates induced by rare gases are smaller in Rb, requiring higher pressures, >10 atm [20], and much smaller in cesium requiring hydrocarbons (methane or ethane) [3]. The heat load associated with this fine-structure relaxation will likely control the beam quality for the DPAL device. Temperature gradients induced by nonuniform optical excitation, wall effects, and fluid transport impose concentration gradients and thus phase variations across the laser beam profile. A full assessment of the system performance requires temperature-dependent rate coefficients for both line-broadening and fine-structure mixing processes. Our broad objective is to unify the DPAL kinetics via interaction potentials [21,22], anchored to asymmetric line shape observations [11,23–25], capable of predicting the temperature-dependent fine-structure mixing rates [16,26]. The maturity of the DPAL kinetic database might then approach that achieved for the HF chemical laser, where well-developed interaction potentials are capable of predicting disposition of reaction exothermicity into rovibrational population distributions [27] and the Schwartz, Slawsky, and Herzfeld (SSH) theory successfully predicts the vibrational-to-transitional energy transfer rates [28].

The spin-orbit mixing rates of alkali-metal atoms in collisions with rare gases have been measured in significant number since the early 1960s [16,18,26,29–50] with a strong effort towards developing a theoretical foundation for predicting the cross sections of nonadiabatic collisions starting much earlier [51–70]. More recently, the experimental focus has shifted to higher-lying Rydberg states, the closely spaced n^2D states, and alkali-metal–alkali-metal collisions [48,50,71–73] and quantum scattering calculations [74,75]. With the dramatic progress in scaling the DPAL power, a resurgence of interest has arisen in the temperature dependence of the fine-structure mixing rates for the lowest ^2P states of K, Rb, and Cs. The broadest experimental study of the temperature-dependent mixing rates were measured almost 50 years ago [16]. Only recently have *ab initio* potentials and a full quantum-mechanical treatment been used to predict temperature dependence of the cross sections [75]. However, strong sensitivity to the interaction potential leads to discrepancies with the observations.

Krause described the interaction between an alkali-metal atom and a rare-gas perturber qualitatively in terms of the Massey parameter, or adiabaticity [33]. The interactions of lithium, sodium, and potassium with both heavy and light rare gases is expected to be nonadiabatic and cannot be treated with Zener's semiclassical calculation [53]. This is in contrast to the Rb and Cs interactions with heavy rare gases, which can be considered adiabatic due to low relative velocity and large spin-orbit splitting. Krause does not further develop this relationship between the adiabaticity and magnitude of the cross section. He does observe that the collisional cross sections do not increase monotonically as might be expected from the polarizability of the rare-gas partner, but rather a dip at neon and then a slow increase to Xe. Gallagher followed up on Krause's work by measuring the temperature dependence of spin-orbit mixing rates for the first-excited P states of Rb and Cs in interactions with the rare gases [16]. He introduces time-dependent perturbation theory to treat the collision of two atoms, but, like Krause, does little to advance this concept further and instead develops and empirical explanation for the trends in the Rb and Cs cross sections in terms of the reduced mass-adjusted temperature [16]. A recent literature review for

[*]Present address: Southern Ohio Council of Higher Education, 3155 Research Blvd, Kettering, Ohio 45420, USA.

[†]Corresponding author: glen.perram@afit.edu

the temperature dependence of the Cs-He, Ar mixing rates suggests a different T^2 to $T^{1/2}$ dependence [74].

Utilizing Krause's idea of adiabaticity [33] along with Nikitin's physical model [64] and Masnou-Seeuws' approach [60], this work develops a theoretical expression for the cross section. We proceed with a development similar to Masnou-Seeuws in that we use a modified interaction potential and a straight-line trajectory in a time-dependent perturbation theory derivation of the energy-transfer probability and drive the model using the cross sections collected from the literature. Organizing the cross sections using adiabaticity reveals all the behavioral trends observed by Gallagher, Krause, and Elward-Berry. The present study provides the theoretical framework for the empirical scaling with adiabaticity we previously reported [76]. Using a single adjustable parameter, the temperature dependence of the fine-structure mixing rates for all alkali-metal excited states induced by rare-gas collisions is developed.

II. REVIEW OF FINE-STRUCTURE MIXING RATES

The fine-structure mixing rates have been measured for Li $(2p)$ [38], Na $(3p)$ [32,35,37], K $(4p)$ [31–33,41], K $(5p)$ [46], Rb $(5p)$ [18,29,33,34], Rb $(6p)$ [40,77], Rb $(7p)$ [40], Cs $(6p)$ [30,33], Cs $(7p)$ [40], and Cs $(8p)$ [36] in collisions with all of the rare gases at a fixed temperature. The temperature dependence of the rates has been measured for the Rb $(6p)$-He, Ne, Ar, Kr, Xe, Cs $(6p)$-He, Ne, and Cs $(7p)$-He, Ne, Ar, Kr, Xe interactions [16,18,78]. We evaluate a total of 203 experimental cross sections from the literature. Pulsed and cw laser-induced fluorescence techniques typically resolve the D_1 and D_2 fluorescence as a function of added buffer gas pressure. Alkali-metal densities are kept below 10^{-5} Torr to prevent self-absorption. Temperature-dependent measurements require increasing the gas temperature without dramatically increasing the alkali-metal density. Observed rate coefficients are divided by the mean relative velocity to provide thermally averaged cross sections for the inelastic collision. Reported uncertainties typically range from 10–50%. Figure 1 provides a summary of the temperature-dependent mixing cross sections for the first-excited P states. The temperatures are scaled by the collision pair reduced mass, μ_{Rg}, relative to the reduced mass of the He–alkali-metal pair, μ_{He}, as originally proposed by Gallagher [16]. This reduced temperature accounts for the different relative velocity distributions of the various rare-gas partners and improves the correlation of the observed cross sections. Several trends are readily identified. First, the cross section for the heavier alkali-metal–rare-gas pairs increases with temperature. Second, Li, Na, and K exhibit much larger, near gas kinetic cross sections. The fine-structure splitting of the first-excited P states are 0.34, 17.2, 57.7, 237.6, and 554 cm^{-1} for Li, Na, K, Rb, and Cs, respectively, and the rates decrease dramatically with larger fine-structure splitting. Finally, for a given alkali metal, the cross sections generally decrease from He to Ne, then increase for the heavier, more polarizable rare gases. While Fig. 1 only shows the values for the first-excited P states for clarity, all measured cross sections roughly decrease by an order of magnitude as the spin-orbit splitting of the alkali metal increases from K to Rb to Cs. While the reduced temperature employed in Fig. 1 organizes the cross sections by alkali metal it fails to organize the data by alkali-metal–rare-gas pairs as the full set of cross sections do not appear to be correlated by the single variable, reduced temperature.

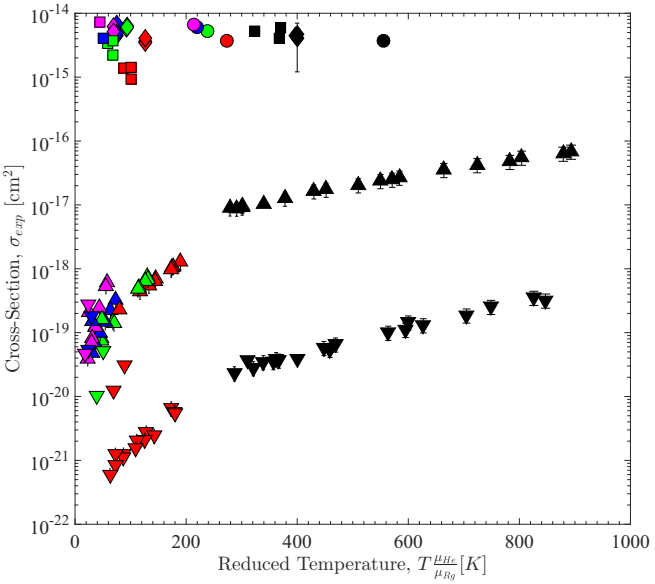

FIG. 1. The experimental cross sections for the fine-structure transition between the first-excited P states are correlated with the reduced temperature. The different alkali metals are given by ○, Li; ◇, Na; □, K; △, Rb; ▽, Cs with the colors corresponding to He (black), Ne (red), Ar (green), Kr (blue), and Xe (magenta). The cross sections have a large decrease as a function of the spin-orbit splitting and a smooth decrease as a function of temperature for a given alkali-metal–rare-gas pair.

For a better correlation to the cross sections, we turn to a modified Massey parameter, or adiabaticity, given by:

$$\xi = \frac{\tau_C}{\tau_N} = \frac{fL}{\bar{v}}, \tag{1}$$

where τ_C is the duration of the collision (atom-atom interaction time), $\tau_N = 1/f$ is the oscillation lifetime defined by the spin-orbit splitting, $\Delta E_{fs} = hf$. The duration of the collision, τ_C may be evaluated as the interaction length, L, relative to the mean velocity of the alkali-metal–rare-gas collision pair, $\bar{v}$.

In addition to the adiabaticity, we define an energy-transfer probability per collision by dividing the experimental cross section, σ_{exp}, by the quantum-defect cross section. The quantum-defect cross section is representative of the hard-sphere cross section where the size of the alkali-metal atom corresponds to the expectation value of the position of the valence electron, defines as

$$\langle r \rangle = a_0 (n^*)^2 \left[1 + \frac{1}{2} \left(1 - \frac{l(l+1)}{(n^*)^2} \right) \right], \tag{2}$$

where l is the orbital angular momentum quantum number. The alkali-metal state is assumed to be described by hydrogenic wave functions, with a_0 as the Bohr radius. The effective quantum number is then defined as

$$n^* = \sqrt{\frac{E_{\text{Ryd}}}{I - E}}, \tag{3}$$

TABLE I. Rare-gas radii (r_{Rg}), in Bohr, derived from viscosity data [79,80] and polarizability (α_{Rg}) [81], in atomic units, are provided.

Rare gas	Radii (r_{Rg}) (Bohr, a_0)	Polarizability (α_{Rg}) $\left(\text{a.u.}, a_0^3\right)$
He	1.68	1.38
Ne	1.99	2.66
Ar	2.81	11.1
Kr	3.19	16.7
Xe	3.75	27.3

where E_{Ryd} is the Rydberg constant and $I - E$ is the energy gap between the level of interest, E, and the ionization potential, I. The quantum-defect cross section is then given by,

$$\sigma_{QD} = \pi(r_{Rg} + \langle r \rangle)^2, \tag{4}$$

where r_{Rg} is the radius of the rare-gas atom as derived from viscosity data [79,80] and summarized in Table II. The probability for population transfer from $^2P_{3/2} \rightarrow {}^2P_{1/2}$ is then given by

$$P = \frac{\sigma_{\text{exp}}}{\sigma_{QD}} = \frac{k_{\text{exp}}}{\bar{v}\sigma_{QD}}, \tag{5}$$

where k_{exp} is the rate coefficient. The values of σ_{QD} used are given in Table I. Using this probability instead of the experimental cross section improves the correlation with adiabaticity and allows comparison directly to the results of the time-dependent perturbation theory calculation developed in Sec. III.

Figure 2 demonstrates that the probabilities for many collision pairs are neatly organized by adiabaticity. While adiabaticity is clearly the primary parameter that controls the probability, it is not the only one. This is apparent in Fig. 2 as only the He and Ne data, excluding the Cs-Ne data, appear to share the same lower bound curve, regardless of alkali-metal collision partner. This curve is well approximated by a power law for the log probability:

$$\ln(P_\xi) = \ln\left(\frac{\sigma_\xi}{\sigma_{QD}}\right) = a - b\xi^c \tag{6}$$

where we refer to P_ξ as the fine-structure mixing probability, σ_ξ as the adiabatic cross section, and the constants' values are $a = 0.76 \pm 0.74$, $b = 3.34 \pm 0.73$, and $c = 0.7784 \pm 0.1$. These fit parameters are improved from our initial scaling report [76] by removing the Cs-Ne interaction, which is enhanced by the Ne polarizability above expected values. This cross section is independent of polarizability and provides a lower bound for the experimental cross section, if the interaction was fully governed by adiabaticity.

Some of the probabilities in Fig. 2 are enhanced above the lower bound of Eq. (6). The degree of enhancement increases with both alkali-metal and rare-gas polarizability, as shown in Fig. 3. The degree of enhancement is characterized by the ratio of the observed cross section to the empirical lower bound of Eq. (6), $\varepsilon = \sigma_{\text{exp}}/\sigma_\xi$. These experimental cross sections vary in temperature for each alkali metal as measurements at the same

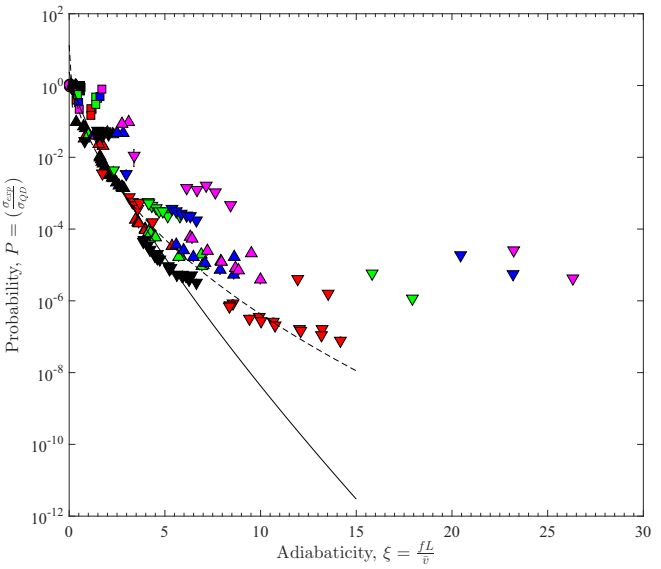

FIG. 2. The probabilities are correlated with the adiabaticity with a fixed interaction length, $L = 5$ Å. The different alkali metals are given by ○, Li; ◇, Na; □, K; △, Rb; ▽, Cs with the colors corresponding to He (black), Ne (red), Ar (green), Kr (blue), and Xe (magenta). The solid curve (–) shown is defined by Eq. (6) and the dashed curve (– –) is the original empirical fit from Ref. [76].

temperature do not exist for all alkali-metal–rare-gas pairs. The temperatures are: 555 K for Li, 400 K for Na, 323 K for K, 340 K for Rb, and 311 K for Cs. The C_6 coefficient determines the strength of the alkali-metal–rare-gas interaction potential,

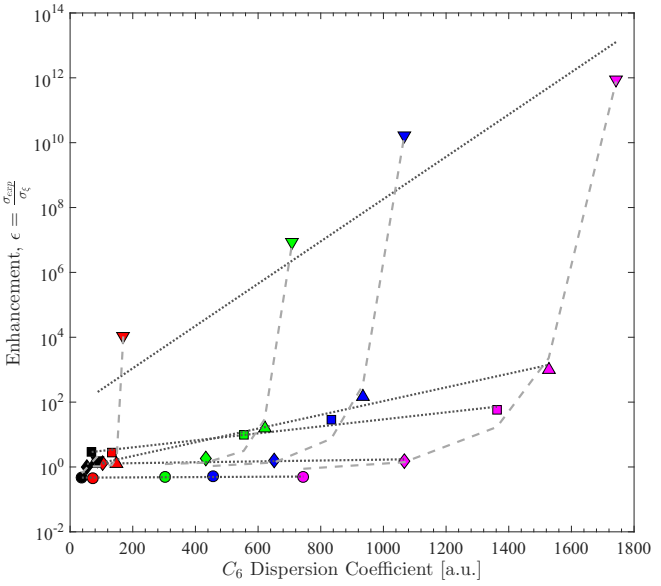

FIG. 3. The enhancement is correlated with the C_6 dispersion coefficient. The different alkali metals are given by ○, Li; ◇, Na; □, K; △, Rb; ▽, Cs with the rare gases filled with the colors corresponding to He (black), Ne (red), A r(green), Kr (blue), and Xe (magenta). A linear fit (· · ·) for each alkali metal shows the deviation in cross section as a function of the rare-gas partner. This is in contrast to the exponential fit (– –), which shows the strong enhancement as a function of the alkali-metal partner.

TABLE II. Quantum-defect cross sections for alkali-metal–rare-gas pairs, $\sigma_{QD}[10^{-15}\text{cm}^2]$.

	He	Ne	Ar	Kr	Xe
Li ($2p$)	3.65	4.01	5.04	5.56	6.37
Na ($3p$)	4.83	5.24	6.41	6.99	7.90
K ($4p$)	5.88	6.33	7.61	8.25	9.23
K($5p$)	24.46	25.38	27.88	29.09	30.91
Rb ($5p$)	6.46	6.93	8.27	8.93	9.95
Rb ($6p$)	26.35	27.30	29.90	31.15	33.03
Rb ($7p$)	73.75	75.33	79.60	81.64	84.67
Cs ($6p$)	7.20	7.70	9.11	9.80	10.87
Cs ($7p$)	28.75	29.74	32.44	33.75	35.71
Cs ($8p$)	79.12	80.76	85.17	87.29	90.42

$V(r) = C_6/r^6$, at large distances and may be evaluated as [82]:

$$C_6 = -e^2\langle r^2\rangle\alpha_{Rg}, \tag{7}$$

where e is the electric charge, α_{Rg} is the rare-gas polarizability from Table II and $\langle r^2\rangle$ is the expectation value of the excited-state alkali-metal atom radius squared obtained using quantum defect theory together with Eq. (3),

$$\langle r^2\rangle = \tfrac{1}{2}(a_0 n^*)^2[5(n^*)^2 + 1 - 3l(l+1)]. \tag{8}$$

A comparison of the empirical C_6 coefficients from the quantum-defect theory and recently calculated values for the ground $X^2\Sigma_{1/2}$, and excited $^2\Pi$ potential energy surfaces correlating with the first excited ^2P states [83,84] are provided in Table III. The quantum-defect C_6 coefficients, defined in Eq. (7), are chosen for this work. These empirical values are used to correct the long-range behavior of *ab initio* potentials in order to match observed line broadening and shifting measurements [24]. Furthermore, this development avoids using any calculated potentials or parameters derived from them so that all alkali-metal excited states can be treated identically, an impossible task using *ab initio* potentials as most calculations focus on the ground and first-excited ^2P states. It is worth noting that the quantum-defect C_6 coefficients are within 25% of the mean of the coefficients for the excited $B^2\Sigma_{1/2}$ and $^2\Pi_{3/2}$ potential energy surfaces. The probability may be further influenced by the positions and depths of shorter-range wells, location and magnitude of avoided crossings, and by interaction length, which is not captured by the correlation in Fig. 3.

The enhancement above the adiabatic cross section increases with both alkali metal and rare gas. The enhancement is modest, $\varepsilon < 100$, except for Rb and Cs, where the rates are indeed very slow. This enhancement is most significant for a given rare gas and weaker for a given alkali metal, implying that the influence of the alkali-metal polarizability is larger than that of the associated rare gas. As with the adiabaticity, if the C_6 coefficient were the only factor we would expect Fig. 3 to show all the data correlated to a single curve dependent on the coefficient. As this is not the case, no empirical scaling law can be formed to correct the adiabatic cross section for the observed increases. Instead, we resort to a time-dependent perturbation theory approach to obtain a theoretical expression for the probability that will be dependent on the interaction potential magnitude, V_0, and the interaction length, L.

III. NONADIABATIC COLLISION THEORY

The ground $X^2\Sigma^+_{1/2}$ potential energy surface for the alkali-metal–rare-gas collision pair correlates to the alkali-metal ground $^2S_{1/2}$ state and the rare-gas ground $^1S_0$ state. The first-excited alkali-metal $^2P_{1/2}$ state and rare-gas $^1S_0$ state yields the $A^2\Pi_{1/2}$ potential energy surface, and the $^2P_{3/2}$ separated atom

TABLE III. Calculated C_6 coefficients, in atomic units, for the ground state, and excited $B^2\Sigma_{1/2}$ and $A^2\Pi$ potential energy surfaces [83,84] are compared to the quantum-defect coefficients given by Eq. (7).

Alkali-metal–rare gas pair	$X^2\Sigma$	Quantum defect	$B^2\Sigma$	$A^2\Pi$	Quantum defect
Li-He	22.51	23.7	50.71	28.27	37.6
Li-Ne	43.79	45.8	98.22	54.92	72.6
Li-Ar	174	190	401.1	220.1	302
Li-Kr	259.6	287	604.9	329.6	456
Li-Xe	410.7	469	972.8	524.4	744
Na-He	25.76	26	76.94	43.74	53.9
Na-Ne	50.41	50.1	149.2	85.11	104
Na-Ar	196.8	209	608.8	341.3	433
Na-Kr	292.7	315	918.7	512	653
Na-Xe	460.9	514	1479	816.7	1070
K-He	39.49	36	103.3	60.85	68.9
K-Ne	77.44	69.6	200.6	118.7	133
K-Ar	299.3	289	812.7	471.7	553
K-Kr	444.1	437	1223	706	835
K-Xe	697.9	713	1964	1123	1360
Rb-He	44.68	38.8	117.8	70.56	77.2
Rb-Ne	88	75	229	137.9	149
Rb-Ar	336.4	312	924.1	545.1	620
Rb-Kr	498	471	1390	815	936
Rb-Xe	780.1	768	2229	1295	1530

yields the two potential energy surfaces, $A^2\Pi_{3/2}$ and $B^2\Sigma_{1/2}$. Collision-induced transitions between the fine-structure split $^2P_{1/2,3/2}$ atomic states occurs primarily due to radial coupling between the $B^2\Sigma_{1/2}$ and $A^2\Pi_{1/2}$ potential energy surfaces. We develop an expression for this fine-structure mixing rate by approximating the collisional dynamics as a straight-line trajectory. Position along the trajectory is expressed as a function of time and used to convert the diabatic coupling potential between the $B^2\Sigma_{1/2}$ and $A^2\Pi_{1/2}$ potential energy surfaces to a time-dependent perturbation. A detailed description of the interaction Hamiltonian and theoretical development may be found in Ref. [85]. First-order perturbation theory is then used to determine the probability per collision for transferring population from the alkali-metal atomic $^2P_{3/2}$ state to the $^2P_{1/2}$ state:

$$P(b,v) = \left| \frac{-i}{\hbar} \int_{-\infty}^{\infty} V(R(t;b,v)) e^{-i\Omega t} dt' \right|^2, \tag{9}$$

where the angular frequency Ω is defined by the fine-structure energy difference, $\Omega = 2\pi f = E_{fs}/\hbar$. The collision trajectory $R(t)$ depends on the initial energy and angular momentum, or impact parameter, b, and relative speed, v. The interaction potential, $V(R)$, is defined by the off-diagonal diabatic potential energy surface matrix elements that couple electronic states in the $^2P_{3/2}$ manifold with electronic states in the $^2P_{1/2}$ manifold [85], but will be approximated by an analytic function developed below. When $V(R(t))$ changes more rapidly than the oscillation represented by $\exp(i\Omega t)$, the collision is sudden and the probability is enhanced. If $V(R(t))$ evolves more slowly, the collision is more adiabatic and the integrand averages to near zero.

The predicted rate coefficient is obtained by the sum over all impact parameters and average over relative speeds:

$$k(T) = 2\pi \int_0^{\infty} bdb \left[4\pi \left(\frac{\mu}{2\pi k_b T} \right)^{3/2} \times \int_0^{\infty} dv \left[v^3 e^{-\frac{\mu v^2}{2k_b T}} P(b,v) \right] \right], \tag{10}$$

where k_b is Boltzmann's constant, μ is the reduced mass of the collision pair, and T is the temperature. The predicted rate coefficient, $k(T)$, can be compared with the experimentally observed, thermally averaged rate coefficient $k_{\exp}(T) = \sigma_{\exp}(T)\bar{v}$, where $\bar{v}$ is the average relative speed.

To calculate the probability we must further develop the radial interaction potential $V(R(t;b,v))$. An approximate form for $V(R(t))$ is taken to be a rectangular Gaussian; a flat-top function with Gaussian onset. The potential evolves during the interaction:

$$V_{RG}(t) = \begin{cases} V_0 e^{-\frac{(t+\tau)^2}{2s^2}} & t < -\tau \\ V_0 & -\tau < t < \tau \\ V_0 e^{-\frac{(t-\tau)^2}{2s^2}} & t > \tau \end{cases} \tag{11}$$

with three parameters: the magnitude of the interaction potential, V_0, the temporal period over which the potential is rapidly changing, s, and the period during which the interaction potential is constant, τ. We assume a straight-line trajectory to relate the interaction length, L, to the interaction period, τ:

$$L^2 = b^2 + v^2\tau^2 \rightarrow \tau = \pm \left[\frac{(L^2 - b^2)}{v^2} \right]^{\frac{1}{2}}. \tag{12}$$

Grazing collisions with $b > L$ yield imaginary τ and are neglected. We note the assumption that s is not a function of velocity and is approximated as $s = \frac{w}{\bar{v}}$ where w is the length scale for the rapidly changing region of the interaction potential. This is consistent with the idea that nearly head-on collisions are the biggest contributors to the probability. A similar approximation is made in the SSH development for vibrational energy transfer [28]. The utility of this approach to modeling the interaction potential is that V_0, L, and w can be estimated from available properties such as polarizability, or a single fine-structure transition rate measurement performed at a single temperature. As a result, fine-structure mixing can be modeled over a wide range of temperatures without explicit knowledge of the *ab initio* potentials. Also, using this approach, the full set of observations is organized by a few parameters, and temperature-dependent rates are predicted from the resulting theory. Validity of the approximate interaction potential will be tested by comparison to the extensive database.

Using Eqs. (11), (12) for $V(t)$ we can arrive at an analytic form for the fine-structure mixing rate, the details of which are only summarized here. See Supplemental Material [86] for the full mathematical derivation. The probability for fine-structure mixing is evaluated from Eq. (10), using Eqs. (11), (12) to obtain:

$$P(b,v) = \left(\frac{2V_0}{\hbar\Omega} \right)^2 [A^2\cos^2(\Omega\tau) + 2AB\cos(\Omega\tau)\sin(\Omega\tau) + B^2\sin^2(\Omega\tau)], \tag{13}$$

where

$$A = \pi^{\frac{1}{2}} \chi e^{-\chi^2},$$
$$B = 1 - \pi^{\frac{1}{2}} \chi e^{-\chi^2} \mathrm{Erfi}(\chi),$$
$$\chi = \frac{\Omega s}{2^{\frac{1}{2}}}. \tag{14}$$

We define χ in terms of the adiabaticity

$$\chi = \frac{s\Omega}{\sqrt{2}} = \frac{(2\pi)}{\sqrt{2}} \frac{fw}{\bar{v}} = \sqrt{2}\pi \frac{w}{L} \xi \tag{15}$$

and integrate the probability over the velocity distribution to yield the analytic expression:

$$P(b,T)\bar{v} = 4\pi \left(\frac{\mu}{2\pi kT} \right)^{\frac{3}{2}} \left(\frac{2V_0}{\hbar\Omega} \right)^2 \left(\frac{kT}{\mu} \right)^2 \times \left[(A^2 + B^2) + (A^2 - B^2)x^2\sqrt{\pi}\mathrm{G}_1(x) + 2AB\sqrt{\pi} \left(x^{\frac{1}{2}}\mathrm{H}_1(x) + \frac{2}{3}\sqrt{\pi}x^2\mathrm{H}_2(x) \right) \right], \tag{16}$$

where $x = \frac{\Omega(L^2 - b^2)\mu}{2kT}$ and G_1, H_1, and H_2 are the Meijer G and generalized hypergeometric functions. The Meijer G function is a further generalization of the generalized

hypergeometric functions and is a generator for most special functions [87]. We further simplify the above expression by noting that both $(A^2 - B^2)x^2\sqrt{\pi}\mathrm{G}_1(x)$ and $2AB\sqrt{\pi}(x^{\frac{1}{2}}\mathrm{H}_1(x) + \frac{2}{3}\sqrt{\pi}x^2\mathrm{H}_2(x))$ rapidly approach zero for values of $\xi > 1$. As most of the alkali-metal adiabaticities are well above this threshold, we proceed by omitting these two terms.

The final step in the calculation is to integrate this probability over the impact parameter. We note that the upper limit to the integral over the impact parameter is reduced to L and as such our perturbation does not account for grazing collisions ($b > L$). This yields the rate

$$k(T) = 8\pi^2\left(\frac{\mu}{2\pi kT}\right)^{3/2}\left(\frac{2V_0}{\hbar\Omega}\right)^2\left(\frac{kT}{\mu}\right)^2(A^2 + B^2)\int_0^L bdb$$
$$= \left(\frac{8\pi^{1/2}}{2^{1/2}\hbar^2}\right)\left(\frac{V_0^2L^2}{\Omega^2}\right)\left(\frac{kT}{\mu}\right)^{1/2}(A^2 + B^2). \quad (17)$$

The rate can then be simplified into the concise form dependent on V_0, L, ξ, and w as

$$k(T) = \frac{V_0^2L^4}{2\pi\hbar^2\bar{v}}\xi^{-2}(A^2 + B^2), \quad (18)$$

where $A^2 + B^2$ can be written in terms of the Dawson integral, $\mathcal{F}(x) = \frac{1}{2}e^{-x^2}\mathrm{Erfi}(x)$ [88],

$$A^2 + B^2 = 2e^{-4\pi^2(\frac{w}{L})^2\xi^2}\pi^3\left(\frac{w}{L}\right)^2\xi^2$$
$$+\left[1 - 2\sqrt{(2)}\pi\frac{w}{L}\xi\mathcal{F}\left(\sqrt{(2)}\pi\frac{w}{L}\xi\right)\right]^2. \quad (19)$$

All of the temperature dependence is contained in the expression $\frac{\xi^{-2}}{\bar{v}}(A^2 + B^2)$. The rest of the term establishes the magnitude of this temperature dependence, which implies that V_0 and L predominantly act as scale factors for the probability whereas ξ, through $\bar{v}$, and w define most of the temperature dependence.

IV. DISCUSSION

Figure 4 shows the results of fitting Eq. (18) to the reviewed literature. These fits were accomplished using a fixed interaction length, L, of 5 Å, a fixed onset width, w, of 3 Å, and an interaction potential magnitude, V_0, left as the only free parameter. The V_0 terms range from 1.3×10^{-5}H for Li $(2p)$-He to 6.2×10^{-3}H for Rb $(5p)$-Xe. The expression for the probability effectively captures the observed temperature dependence of the probabilities in spite of the fixed parameters for all the alkali-metal–rare-gas pairs. The mean error is ≈65%, close to the maximum experimental errors of 50% but less than the scatter between distinct measurements of nearly 100%. Given a single measurement for an alkali-metal–rare-gas pair to fix V_0, Eq. (18) has the ability to predict the temperature dependence for that pair to within a factor of two of the measurement error. If the C_6 coefficient is a sufficient surrogate for V_0 then one might expect the two to be closely correlated. We see in Fig. 5 that this is not necessarily true. In fact, V_0 trends similarly to the enhancement probability shown in Fig. 3. This is expected as V_0 is the free parameter

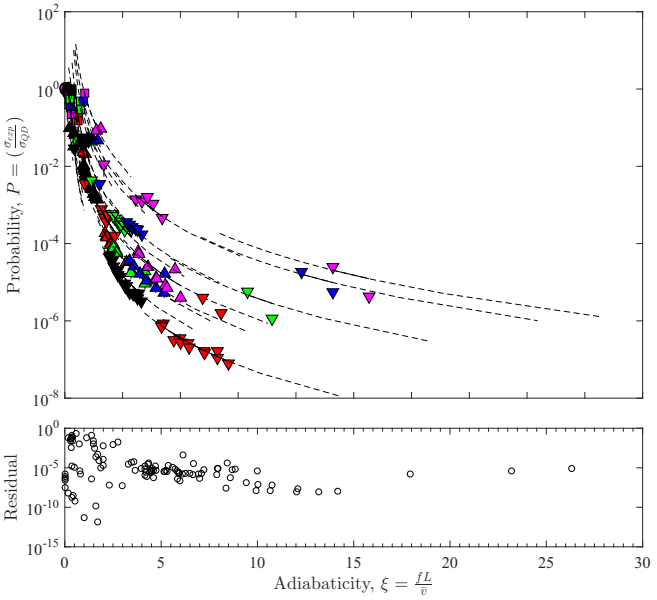

FIG. 4. The experimentally measured cross sections normalized to the quantum-defect cross section are shown as a function of adiabaticity where ○, Li; ◇, Na; □, K; △, Rb; ▽, Cs with the colors corresponding to He (black), Ne (red), Ar (green), Kr (blue), and Xe (magenta). Residuals of 0.5 correspond to errors of 65%. The symbols are defined by Eq. (5) and the dashed line (−−) represents the theoretical prediction, $P(T) = k(T)/(\sigma_{QD}\bar{v})$ where $k(T)$ is given by Eq. (18). The displayed prediction corresponds to a temperature range of 100–1000 K. V_0 values range from 1.3×10^{-5} H for Li $(2p)$-He to 6.2×10^{-3} H for Rb $(5p)$-Xe.

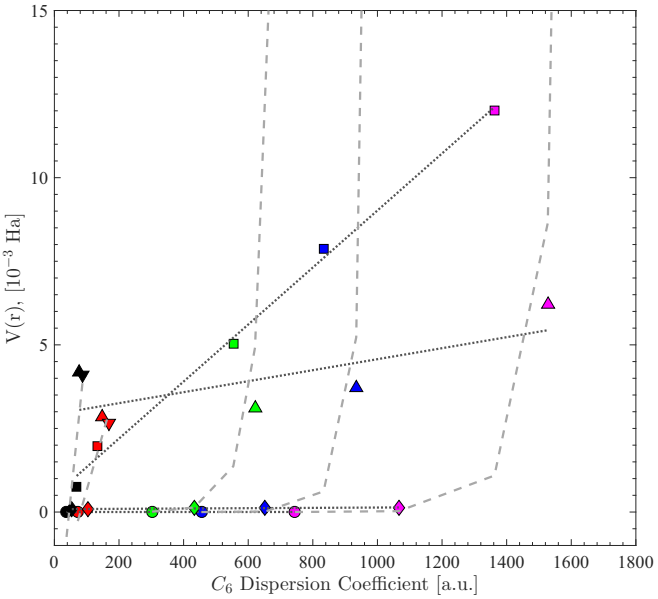

FIG. 5. V_0 are plotted against the quantum-defect C_6 coefficients. The different alkali metals are given by ○, Li; ◇, Na; □, K; △, Rb; ▽, Cs with the colors corresponding to He (black), Ne (red), Ar (green), Kr (blue), and Xe (magenta). A linear fit (· · ·) for each alkali metal shows the deviation in cross section as a function of the rare-gas partner. This is in contrast to the exponential fit (−−), which shows the strong deviation as a function of the alkali-metal partner.

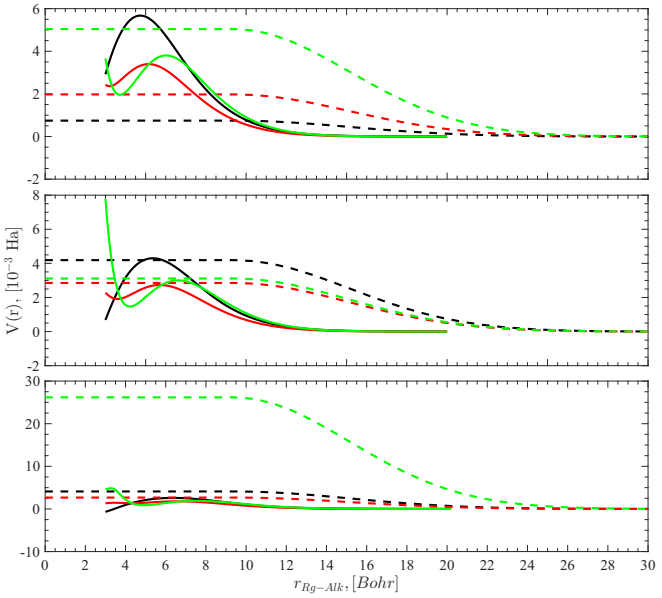

FIG. 6. The theoretical (–) and predicted (−−) potentials for collisions of K (top), Rb (middle), Cs (bottom) in collisions with He (black), Ne (red), and Ar (green) [21]. The predicted potentials are shallower and wider than the *ab initio* potentials.

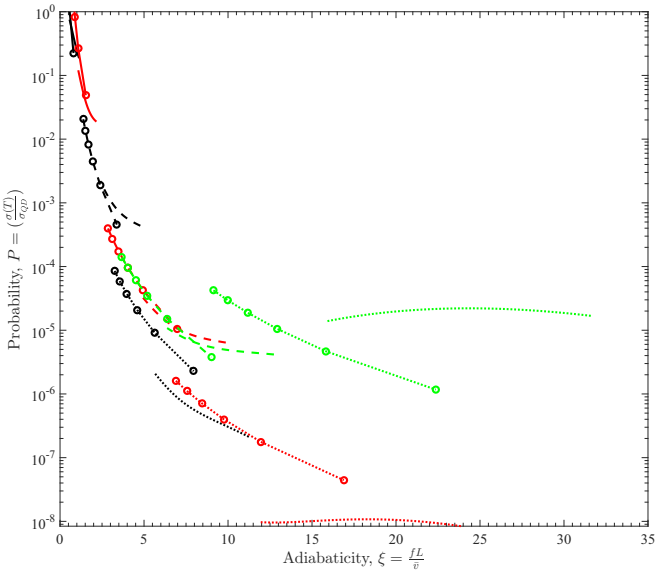

FIG. 7. The prediction of Eq. (18) is shown as a line with circle markers corresponding to a temperature range of 100–1000 K. The lines without markers correspond to full quantum-mechanical calculations of the cross sections conducted by Lewis *et al.* [75]. The different line types correspond to K (–), Rb (- -), and Cs (· · ·) and with colors corresponding to He (black), Ne (red), and Ar (green).

designed to account for just that dependence. There is one significant deviation between the dependencies of V_0 and the enhancement probability on the C_6 coefficient. The predicted V_0 for the Cs-Ar, Kr, and Xe interactions are anomalously high and have been excluded from Fig. 5. These cross sections are significantly higher than expected, likely due to a mechanism beyond a simple binary collision modeled in this work. A thorough discussion on the sources of measurement error associated with the Cs–rare-gas cross sections are provided in a recent review of Cs energy-transfer measurements [74]. Ignoring the scale of the Cs-Ar, Kr, Xe data, we see that both V_0 and the enhancement probability show the same exponential dependence on alkali-metal polarizability for a given rare gas as well as a linear dependence on rare-gas polarizability for a given alkali metal.

The potentials for the alkali-metal–rare-gas interaction have been calculated at the spin-orbit multireference configuration interaction level by Blank *et al.* for K, Rb, Cs in collisions with He, Ne, and Ar [21]. Figure 6 shows the calculated diabatic potential energy surfaces compared to the current model predicted potentials. The long-range (>10 Bohr) form of the model and the calculated potentials are remarkably similar with the predicted potentials decreasing slower due to the large onset width, w. One major deviation between the *ab initio* potentials and the current modeled forms exist for the Cs-Ar case where the modeled potential is significantly higher in energy, likely driven by the aforementioned three-body effects. In the short range (<10 Bohr), the *ab initio* potential vary more drastically from their modeled counterparts. This is driven by the complex interaction of the alkali-metal–rare-gas that is overly simplified by our proposed potential structure designed to maintain an analytic form. The current predicted mixing rates are similar to the probabilities computed using a time-dependent wave packet approach [75], as seen in Fig. 7. These calculated quantum-mechanical probabilities for the K and Rb cases agree with the predicted temperature dependence predominantly at higher temperatures. The low-temperature behavior is underestimated in the full quantum-mechanical development. The Cs-He prediction is closest in temperature dependence but underestimates the overall probabilities by an order of magnitude. The Cs-Ne and Cs-Ar probabilities are also off by approximately an order of magnitude. It is also worth noting that the Cs-Ar prediction is substantially higher than the Cs-Ne prediction, which is consistent with our anomalously high V_0. These higher-fidelity theoretical calculations are very sensitive to the *ab initio* potential energy surfaces, with accuracy less than $10\,\mathrm{cm}^{-1}$ required for collision-induced shifts [11,21]. The advantage of the current semiclassical calculation with approximate potential energy surfaces is the development of a broadly applicable scaling law with only a few empirical parameters.

As an example of the predicted temperature-dependent rates, we turn to evaluating the $5^2P_{3/2} \rightarrow 5^2P_{1/2}$ mixing cross section for the Rb-He DPAL system. Figure 8 compares the most comprehensive experimental observations for the temperature dependence [16] with the current prediction. Gallagher's very early work [16] remains the best reported temperature -dependent values. His fit to the observations employed a two-term temperature dependence:

$$Q(T) = \Sigma_{i=1}^{2} K_i \Gamma(n_i + 2)\left(\frac{2kT}{\mu v_0^2}\right)_i^n, \qquad (20)$$

where $K_1 = 3.4\times10^{-20}\mathrm{cm}^2$, $K_2 = 490\times10^{-20}\mathrm{cm}^2$, $n_1 = 3$, $n_2 = 0.5$, and $v_0 = 10^5\mathrm{cm/sec}$. At $T = 400$ K, the mixing rate is $k = 1.92\times10^{-12}\mathrm{cm}^3/\mathrm{at.\,s}$, increasing to

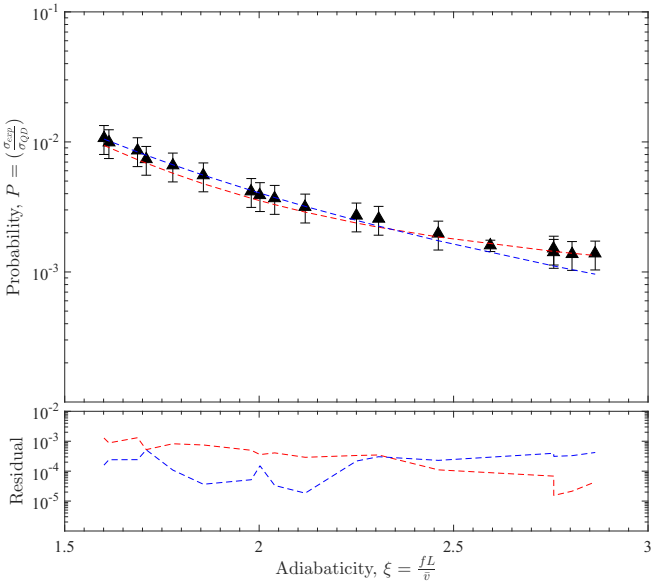

FIG. 8. Equations (20) and (21) are compared to the Rb-He probabilities. Gallagher's empirical model, Eq. (20), is represented by the dashed red curve and the current model, Eq. (21), is represented by the dashed blue line. Both models agree to within 30%.

2.99×10^{-12}cm^3/at. s at 500 K. At 20 atmospheres of He at 400 K, the mixing time is 1.42 ns, or 18.5 cycles per radiative lifetime (26 ns). The current prediction for the rate coefficient, using the recommended values $L = 0.5$ nm, $w = 0.3$ nm, and $V_0 = 4.19\times10^{-3}$H is:

$$k(T) = 5.58\times10^{-16}\sqrt{T}\left(\frac{51089}{T}e^{-32524/T} + \left(1-\frac{226}{\sqrt{T}}e^{-16262/T}\mathrm{Erfi}\left(\frac{127.523}{\sqrt{T}}\right)\right)^2\right), \quad (21)$$

where T is the temperature in Kelvin. This yields the second curve in Fig. 8. The two rates agree to within 30% across the temperature range 279–893 K with our prediction yielding more accurate results for temperatures above 400 K. We prefer the current result, as the full alkali-metal–rare-gas database is unified with Eq. (18). It is worth noting that at elevated pressures, three-body collisions enhance the rate, Rb-He $k_{3b} = 1.19\times10^{-32}$cm^6/at.^{2} s [18].

V. CONCLUSION

The experimental spin-orbit mixing cross sections have been collected from the literature and reviewed in terms of the adiabaticity and rare-gas interaction. The data show a consistent trend for He, and most of the Ne, probabilities with a positive enhancement from that trend as a function of polarizability. Using an approximate square-Gaussian effective potential and a straight-line trajectory in a time-dependent perturbation theory development, an analytic expression for the probability of energy transfer in alkali-metal–rare-gas collisions has been derived. The expression is dependent on the magnitude of the effective potential, V_0, the flat top distance, L, and the onset width of the Gaussian w. A fixed L and w of 5 Å and 3 Å, respectively, are suitable for matching the complete alkali-metal database. The temperature dependence for any alkali-metal–rare-gas cross section can be extracted from the provided expression if V_0 is used to set the magnitude of the curve. There is good agreement between the analytic model and the full quantum-mechanical development at high temperatures for K and Rb but the data and analytic model show a steeper trend with decreasing temperature than the full numerical approach predicts.

Further testing of this model is required, especially in the nonadiabatic cases of Li, Na, and K as well as the extremely adiabatic cases of Cs-Ar, Kr, Xe where temperature-dependent rate coefficients have not yet been measured. The formulation may also apply to the mixing of the Halogens for the $^2P_{1/2} \rightarrow {}^2P_{3/2}$ transition. However, additional temperature-dependent rate measurements will be required. The halogens would be a particularly interesting case as the spin-orbit splittings range from 400 cm^{-1} in fluorine to 7600 cm^{-1} in iodine, which corresponds to adiabaticities of 4.3 (F-He) to 360 (I-Xe) at 300 K, a much wider range than in the alkali-metal–rare-gas collision of $\xi = 0.0024$–26.3.

ACKNOWLEDGMENT

This work was partially funded by the High Energy Laser Joint Technology Office.

[1] W. F. Krupke, R. J. Beach, V. K. Kanz, and S. A. Payne, Opt. Lett. **28**, 2336 (2003).
[2] G. P. Perram, S. J. Cusumano, S. T. Fiorino, and R. L. Hengehold, *An Introduction to Laser Weapon Systems* (Directed Energy Professional Society, Albuquerque, 2010).
[3] A. V. Bogachev, S. G. Garanin, A. M. Dudov, V. A. Eroshenko, S. M. Kulikov, G. T. Mikaelian, V. A. Panarin, V. O. Pautov, A. V. Rus, and S. A. Sukharev, Quantum Electron. **42**, 95 (2012).
[4] G. A. Pitz, D. M. Stalnaker, E. M. Guild, B. Q. Oliker, P. J. Moran, S. W. Townsend, and D. A. Hostutler, Proc. SPIE **9729**, 972902 (2016).
[5] E. J. Hurd, J. C. Holtgrave, and G. P. Perram, Opt. Commun. **357**, 63 (2015).
[6] C. V. Sulham, G. P. Perram, M. P. Wilkinson, and D. A. Hostutler, Opt. Commun. **283**, 4328 (2010).
[7] W. S. Miller, C. V. Sulham, J. C. Holtgrave, and G. P. Perram, Appl. Phys. B **103**, 819 (2011).
[8] G. D. Hager and G. P. Perram, Appl. Phys. B **101**, 45 (2010).
[9] G. D. Hager and G. P. Perram, Appl. Phys. B **112**, 507 (2013).
[10] B. D. Barmashenko, S. Rosenwaks, and M. C. Heaven, Opt. Commun. **292**, 123 (2013).

[11] W. S. Miller, C. A. Rice, G. D. Hager, M. D. Rotandaro, H. Berriche, and G. P. Perram, J. Quant. Spectrosc. Radiat. Transf. **184**, 118 (2016).
[12] G. A. Pitz, C. D. Fox, and G. P. Perram, Phys. Rev. A **82**, 042502 (2010).
[13] M. D. Rotandaro and G. P. Perram, J. Quant. Spectrosc. Radiat. Transf. **57**, 497 (1997).
[14] G. A. Pitz, D. E. Wertepny, and G. P. Perram, Phys. Rev. A **80**, 062718 (2009).
[15] M. V. Romalis, E. Miron, and G. D. Cates, Phys. Rev. A **56**, 4569 (1997).
[16] A. Gallagher, Phys. Rev. **172**, 88 (1968).
[17] G. A. Pitz, C. D. Fox, and G. P. Perram, Phys. Rev. A **84**, 032708 (2011).
[18] J. F. Sell, M. A. Gearba, B. M. Patterson, D. Byrne, G. Jemo, T. C. Lilly, R. Meeter, and R. J. Knize, J. Phys. B: At., Mol. Opt. Phys. **45**, 055202 (2012).
[19] M. D. Rotondaro and G. P. Perram, Phys. Rev. A **57**, 4045 (1998).
[20] S. S. Wu, T. F. Soules, R. H. Page, S. C. Mitchell, V. K. Kanz, and R. J. Beach, Opt. Commun. **281**, 1222 (2008).
[21] L. Blank, D. E. Weeks, and G. S. Kedziora, J. Chem. Phys. **136**, 124315 (2012).
[22] J. Dhiflaoui and H. Berriche, J. Phys. Chem. A **114**, 7139 (2010).
[23] L. Blank and D. E. Weeks, Phys. Rev. A **90**, 022510 (2014).
[24] G. D. Hager, G. E. Lott, A. J. Archibald, L. Blank, D. E. Weeks, and G. P. Perram, J. Quant. Spectrosc. Radiat. Transf. **147**, 261 (2014).
[25] K. A. Kluttz, T. D. Averett, and B. A. Wolin, Phys. Rev. A **87**, 032516 (2013).
[26] M. A. Gearba, J. F. Sell, B. M. Patterson, R. Lloyd, J. Plyler, and R. J. Knize, Opt. Lett. **37**, 1637 (2012).
[27] G. C. Manke II and G. D. Hager, J. Phys. Chem. Ref. Data **30**, 713 (2001).
[28] J. Yardley, *Introduction to Molecular Energy Transf.* (Elsevier, Netherlands, 2012).
[29] T. J. Beahn, W. J. Condell, and H. I. Mandelberg, Phys. Rev. **141**, 83 (1966).
[30] M. Czajkowski, D. A. McGillis, and L. Krause, Can. J. Phys. **44**, 91 (1966).
[31] G. D. Chapman and L. Krause, Can. J. Phys. **44**, 753 (1966).
[32] J. A. Jordan and P. A. Franken, Phys. Rev. **142**, 20 (1966).
[33] L. Krause, Appl. Opt. **5**, 1375 (1966).
[34] B. Pitre, A. G. A. Rae, and L. Krause, Can. J. Phys. **44**, 731 (1966).
[35] J. Pitre and L. Krause, Can. J. Phys. **45**, 2671 (1967).
[36] M. Pimbert, J. Phys. France **33**, 331 (1972).
[37] J. Pascale and R. E. Olson, J. Chem. Phys. **64**, 3538 (1976).
[38] J. Elward-Berry and M. J. Berry, J. Chem. Phys. **72**, 4500 (1980).
[39] M. Hugon, F. Gounand, P. R. Fournier, and J. Berlande, J. Phys. B: At. Mol. Phys. **13**, 1585 (1980).
[40] P. Munster and J. Marek, J. Phys. B: At. Mol. Phys. **14**, 1009 (1981).
[41] J. M. Mestdagh, J. Berlande, J. Cuvellier, P. de Pujo, and A. Binet, J. Phys. B: At. Mol. Phys. **15**, 439 (1982).
[42] J. Wolnikowski, J. B. Atkinson, J. Supronowicz, and L. Krause, Phys. Rev. A **25**, 2622 (1982).
[43] B. G. Zollars, H. A. Schuessler, J. W. Parker, and R. H. Hill, Phys. Rev. A **28**, 1329 (1983).
[44] J. Supronowicz, J. B. Atkinson, and L. Krause, Phys. Rev. A **30**, 112 (1984).
[45] J. Supronowicz, J. B. Atkinson, and L. Krause, Phys. Rev. A **31**, 2691 (1985).
[46] R. Berends, W. Kedzierski, and L. Krause, J. Quant. Spectrosc. Radiat. Transf. **37**, 157 (1987).
[47] T. R. Mallory, W. Kedzierski, J. B. Atkinson, and L. Krause, Phys. Rev. A **38**, 5917 (1988).
[48] I. Jackowska and M. Lukaszewski, J. Phys. B: At., Mol. Opt. Phys. **23**, 2097 (1990).
[49] M. Lukaszewski and I. Jackowska, J. Phys. B: At., Mol. Opt. Phys. **24**, 2047 (1991).
[50] B. Bieniak, K. Fronc, S. Gateva-Kostova, M. Głódź, V. Grushevsky, J. Klavins, K. Kowalski, A. Rucińska, and J. Szonert, Phys. Rev. A **62**, 022720 (2000).
[51] M. P. Langevin, Ann. Chim. Phys. **5**, 245 (1905).
[52] L. D. Landau, Phys. Z. Sowjetunion **2**, 7 (1932).
[53] C. Zener, Phys. Rev. **38**, 277 (1931).
[54] N. Scheel and V. Griffing, J. Chem. Phys. **36**, 1453 (1962).
[55] E. E. Nikitin, J. Chem. Phys. **43**, 744 (1965).
[56] E. E. Nikitin, Opt. Spectrosc. **22**, 379 (1967).
[57] E. I. Dashevskaya and E. E. Nikitin, Opt. Spectrosc. **22**, 473 (1967).
[58] H. Hooymayers and C. Alkemade, Chem. Phys. Lett. **4**, 277 (1969).
[59] R. H. G. Reid and A. Dalgarno, Phys. Rev. Lett. **22**, 1029 (1969).
[60] F. Masnou-Seeuws, J. Phys. B **3**, 1437 (1970).
[61] E. I. Dashevskaya, E. E. Nikitin, and A. I. Reznikov, J. Chem. Phys. **53**, 1175 (1970).
[62] F. Masnou-Seeuws and R. McCarroll, J. Phys. B **7**, 2230 (1974).
[63] R. K. Preston, C. Sloane, and W. H. Miller, J. Chem. Phys. **60**, 4961 (1974).
[64] E. Nikitin, in *Advances in Chemical Physics, Volume 28: The Excited State in Chemical Physics* (Wiley, New York, 1975), Chap. V, pp. 317–378.
[65] R. E. Olson, Chem. Phys. Lett. **33**, 250 (1975).
[66] R. H. G. Reid, J. Phys. B **8**, L493 (1975).
[67] M. B. Faist and R. B. Bernstein, J. Chem. Phys. **64**, 2971 (1976).
[68] J. Pascale and P. M. Stone, J. Chem. Phys. **65**, 5122 (1976).
[69] R. H. G. Reid and R. F. Rankin, J. Phys. B **11**, 55 (1978).
[70] J. B. Delos, Rev. Mod. Phys. **53**, 287 (1981).
[71] M. Lukaszewski and I. Jackowska, J. Phys. B **21**, L659 (1988).
[72] N. P. Wells, T. U. Driskell, and J. C. Camparo, Phys. Rev. A **92**, 022505 (2015).
[73] T. L. Correll, V. Horvatic, N. Omenetto, J. D. Winefordner, and C. Vadla, Spectrochim. Acta, Part B **61**, 623 (2006).
[74] C. Vadla, V. Horvatic, and K. Niemax, Spectrochim. Acta, Part B **58**, 1235 (2003).
[75] C. D. Lewis, II, Ph.D. thesis, Air Force Institute of Technology, 2011.
[76] B. Eshel, D. E. Weeks, and G. P. Perram, Proc. SPIE **8962**, 896207 (2014).
[77] I. Siara, E. S. Hrycyshyn, and L. Krause, Can. J. Phys. **50**, 1826 (1972).
[78] I. N. Siara, H. S. Kwong, and L. Krause, Can. J. Phys. **52**, 945 (1974).
[79] H. L. Johnston and E. R. Grilly, J. Phys. Chem. **46**, 948 (1942).

[80] H. J. M. Hanley, J. Phys. Chem. Ref. Data **2**, 619 (1973).
[81] N. Allard and J. Kielkopf, Rev. Mod. Phys. **54**, 1103 (1982).
[82] W. R. Hindmarsh and J. M. Farr, *Collision Broadening of Spectral Lines by Neutral Atoms* (Pergamon Press, Oxford, 1972).
[83] J.-Y. Zhang and J. Mitroy, Phys. Rev. A **76**, 022705 (2007).
[84] J. Mitroy and J.-Y. Zhang, Phys. Rev. A **76**, 032706 (2007).
[85] J. A. Cardoza, Master's thesis, Air Force Institute of Technology, 2015.
[86] See Supplemental Material at http://link.aps.org/supplemental/10.1103/PhysRevA.95.042708 for detailed calculation of the time-dependent perturbation theory.
[87] H. Bateman, W. Magnus, F. Oberhettinger, and F. G. Tricomi, in *Higher Transcendental Functions*, edited by A. Erdélyi (McGraw-Hill, New York, 1953), Vol. 1.
[88] M. Abramowitz and I. A. Stegun, *Handbook of Mathematical Functions With Forumlas, Graphs, and Mathematical Tables*, 10th ed. (National Bureau of Standards, Washington, DC, 1972).